Fatigue resistance of rib to deck, crossbeam to deck and deck to deck welds in orthotropic decks using structural stress

Maljaars, Johan; Pijpers, Richard; Wu, Weijian; Kolstein, Henk

DOI
10.1016/j.ijfatigue.2023.107742

Publication date
2023

Document Version
Final published version

Published in
International Journal of Fatigue

International Journal of Fatigue 175 (2023) 107742

Contents lists available at ScienceDirect

International Journal of Fatigue

journal homepage: www.elsevier.com/locate/ijfatigue

Fatigue resistance of rib to deck, crossbeam to deck and deck to deck welds in orthotropic decks using structural stress

Johan Maljaars [a,b,*], Richard Pijpers [a], Weijian Wu [c,d], Henk Kolstein [c]

[a] TNO, Molengraaffsingel 8, Delft, The Netherlands
[b] Eindhoven University of Technology, Blauwe Zaale 1, Eindhoven, The Netherlands
[c] Delft University of Technology, Mekelweg 5, Delft, The Netherlands
[d] Technical University of Denmark (DTU), Brovej 118, Lyngby, Denmark

ARTICLE INFO

Keywords:
Orthotropic bridge deck
Fatigue tests
Hot-spot stress
FAT class
TS 1993-1-901

ABSTRACT

This study derives the fatigue resistance of welded details in orthotropic decks using structural stress (hot-spot stress where possible) based on tests described in literature and tests by the authors. The data are supported with linear elastic fracture mechanics simulations. Details covered are the rib to deck weld, the crossbeam to deck weld and the deck butt weld. High fatigue resistances are found, caused by favourable loading modes (bending and compression) and reduced driving force with the growth of cracks. The technical specification TS 1993-1-901, part of the new generation of Eurocodes, is based on the results of this study.

1. Introduction

Steel Orthotropic Bridge Deck (OBD) structures are widely used in bridge construction, mainly because of their high ratio between load carrying capacity and self-weight. Most modern OBD in road bridges consist of a deck plate supported by trapezoidal-shaped ribs in longitudinal (i.e., traffic flow) direction and supported by crossbeams – also called floor beams – in transverse direction. Experience from practice reveals that OBD structures are sensitive to fatigue deterioration, often dominating the service life. Studies into the fatigue performance have been published since the years 1960 and 1970 [1–3] and this continues to–date [4,5]. These studies have resulted in guidelines and standards for the fatigue design of OBD. The European standard EN 1993-2 [6] contains an informative annex with geometrical design recommendations for OBD, aiming at preventing fatigue cracks during the design life. The European standard EN 1993-1-9 [7], the updated version thereof [8] and the American AASHTO LRFD design specifications [9] give tables of the fatigue resistance of various details in OBD, enabling engineers to design OBD for a certain (bridge) application. The IIW recommendations for fatigue design of welded joints [10], the recommended practice DNV-RP-C203 [11] and the British Standard BS 7608 [12] provide the fatigue resistance of a limited number of all fatigue sensitive details in OBD.

The fatigue resistance of OBD details in the aforementioned guidelines and standards refers to the nominal (i.e., far-field) stress as the basis. Analyses with the Finite Element Method (FEM) show that large stress gradients are present in the vicinity of many welds in OBD, causing problems in the application of the nominal stress method. Some fatigue-sensitive details, such as the crack in the deck plate at the junction of the rib to deck and the crossbeam to deck weld [13], are not covered in [7,8] because the nominal stress is undefined. Similarly, fatigue tests are often evaluated using measured strains [14], but the locations of the strain gauges vary between the older test series, causing inconsistencies in the fatigue resistance.

Alternatives to the nominal stress method are available that are better suited for details with large stress gradients. Many recent studies on OBD details use a structural or a local stress parameter as the reference for the fatigue resistance of OBD details, such as the hot-spot stress method [15–17], the traction stress method [18–20] and the effective notch stress method (ENM) [21–23]. The hot-spot stress method is able to consider the stress gradient effect, but it is less local than the ENM, implying that it is not affected by the geometry of the weld profile. It is also less laborious for practitioners than the traction stress method and the ENM. This paper evaluates the fatigue resistance of details in or near the rib to deck welds, the crossbeam to deck welds and the deck butt welds using structural stress – the hot-spot stress where possible or an equivalent weld stress for cracks through the weld. A second paper evaluates the fatigue resistance of the crossbeam to rib and rib to rib connections. Together, they form the background of a new Technical Specification TS 1993-1-901 [24] 'Fatigue design of OBD with the hot-spot stress method' that will become part of the new generation of Eurocodes.

* Corresponding author at: Eindhoven University of Technology, Blauwe Zaale 1, Eindhoven, The Netherlands.
E-mail address: johan.maljaars@tno.nl (J. Maljaars).

https://doi.org/10.1016/j.ijfatigue.2023.107742
Received 13 March 2023; Received in revised form 20 May 2023; Accepted 23 May 2023
Available online 1 June 2023

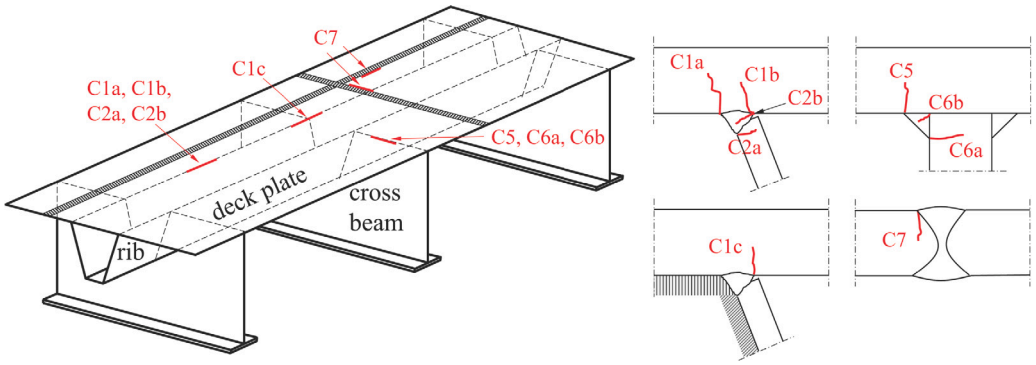

Fig. 1. Overview of details discussed in this paper.

2. Methods and structural details considered

Fig. 1 gives an overview of the fatigue sensitive details discussed in this paper. Each detail is considered individually, starting from the as-welded (i.e., uncracked) state. The detail designation corresponds with that in TS 1993-1-901 [24]. The hot-spot stress method obtained from surface extrapolation [10,11] can be straightforwardly applied to all weld toe details (C1a, C2a, C5, C6a and C7). For relatively coarse meshes composed of elements with quadratic shape function, the hot-spot stress σ_{hs} is:

$$\sigma_{hs} = 1.5\sigma_{0.5t} - 0.5\sigma_{1.5t} \tag{1}$$

where $\sigma_{0.5t}$ and $\sigma_{1.5t}$ are the stresses at the plate surface $0.5t$ and $1.5t$ away from the weld toe, respectively, where t is the plate thickness. The nominal stress is used for weld failure of double load carrying fillet welds. Following prEN 1993-1-9 [8], this stress is determined as:

$$\sigma_{wf} = \frac{F}{2a_w} + \frac{M}{{a_w}^2 + a_w t} \tag{2}$$

where a_w is the weld throat, F is the normal force per unit length and M is the bending moment per unit length. Note that the force-pair method used in Eq. (2) to estimate the fatigue relevant weld stress caused by a bending moment is conservative [25].

A typical detail in OBD with trapezoidal ribs is the single sided partial penetration weld with cracks initiating at the root of the weld, either at the deck plate side (Detail C1b) or at the weld side (Detail C2b). In agreement with [26] the former crack location is evaluated with the hot-spot stress method at the bottom side of the deck plate inside the rib, see Fig. 2(b). The stress in the rib web governs the latter crack location. From a theoretical perspective, the weld throat and the eccentricity between the weld and the rib web influence the stress distribution in the weld. The authors propose the following equation for the weld root stress of the single sided weld (Detail C2b):

$$\sigma_{wf} = \frac{F}{a_w} + \frac{6}{{a_w}^2}(M + Fe) \tag{3}$$

where eccentricity e is defined in Fig. 2(c). The appropriateness of this equation will be verified by comparison with the ENM in the next section.

Fatigue test data are collected from literature to evaluate the fatigue resistance. A limited number of data or even no data are found for some details, e.g., for manual overhead welds. Fatigue tests are performed by the authors in such cases. In addition, linear elastic Fracture Mechanics (FM) simulations are carried out to support the fatigue resistance of the tests, or to evaluate the fatigue performance in case of thick deck plates. The Appendix describes the FM model and its validation with fatigue tests.

The data are evaluated for the number of cycles N causing a visually observed crack with a through-thickness length in the order of a few cm or a surface crack with a height of at least 75% of the plate thickness for the full deck tests, and a visually observed crack length in the order of a few cm or complete failure for the component (small specimen) tests. If available, the detail specific criteria are given in the subsequent section. In agreement with most standards on fatigue, this number of cycles is fitted with a Basquin relation as a function of the stress range $\Delta\sigma$:

$$\log_{10} N = C + m \log_{10} \Delta\sigma \tag{4}$$

where C is a detail dependent factor that is assumed to be normal distributed and $m = -3$ (fully informative prior for welded joints). Run-outs are ignored in the fit. In agreement with the derivations for other details in EN 1993-1-9 [7], the fatigue reference resistance $\Delta\sigma_C$ is defined as the stress range at which the detail survives 2 million cycles with a 95% prediction bound [27,28]. It follows from a least-square fit of C as proposed by [29].

The fatigue reference resistance using the hot-spot stress method is 90 MPa or 100 MPa for load carrying fillet welds or other welds, respectively, of standard details [7,10]. The fatigue reference resistance is 40 MPa for load carrying fillet welds with weld root cracks. However, fatigue tests show that the actual resistance is much higher for many details in OBD. Reasons are:

- The tests on which the reference resistances of 90 MPa and 100 MPa are based, are loaded in tension–tension mode with relatively high stress ratios. Many details in OBD are loaded in bending, often with compression at the crack initiation location. Even though residual welding stresses are present, external compression is reported as positively influencing the fatigue resistance [30].
- OBD structures are generally redundant and tolerable to fatigue cracks. Adjacent elements take over part of the load in case a crack causes loss in flexural rigidity. In some details, a crack initiates at a location of high traffic-induced stress (at which the hot-spot stress is computed) but, after some growth, it enters an area with lower stress (for which the computed hot-spot stress is not representative), giving a reduced crack driving force. In addition, the load is multi-directional for some details and the crack mode is not always Mode I [31]. This influences the crack growth rate, which is usually reported as relatively low in tests of OBD details.
- The reference resistances of weld toe cracks of 90 MPa and 100 MPa are given for a plate thickness of 25 mm. Many elements in OBD are thinner than 25 mm, down to 6 mm for most ribs. A beneficial thickness effect may then arise. Sonsino et al. [32] demonstrate that the S–N curves of welded details in thin plates is 'flatter' (with a higher slope parameter) as compared to thicker plates. This is also observed in some OBD details. Nonetheless, the fatigue resistances are conservatively based on the standard slope parameter of $m = -3$ for ease of use.

The specific fatigue resistance of OBD details deviating from the standard resistance values is the motivation of studying the fatigue resistance per detail here. Most other papers use a single or a limited

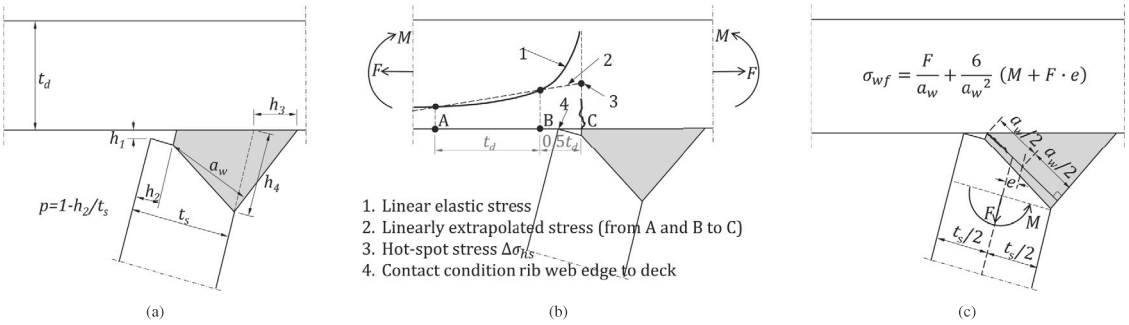

Fig. 2. Rib to deck weld: (a) Geometrical definitions; (b) Hot-spot stress definition for deck plate cracks from the weld root; (c) Weld stress definition for weld cracks from the weld root.

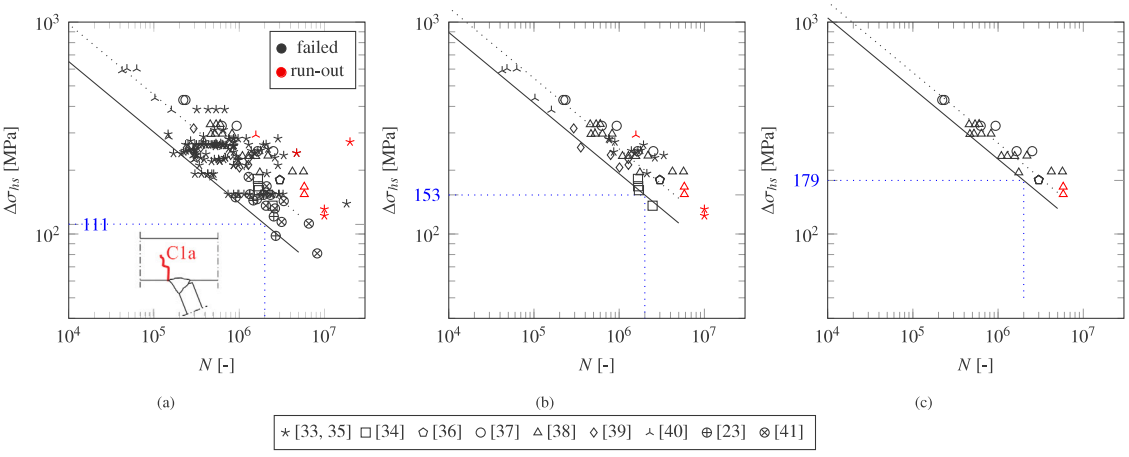

Fig. 3. Fatigue of Detail C1a, sources [23,33–41]: (a) All data; (b) Selection $R < 0$, $p \geq 0.7$ and 10 mm $\leq t_d \leq$ 19 mm; (c) Selection $R < 0$, $p \geq 0.7$ and $t_d = 10$ or 12 mm.

number of test series of OBD details. The authors of the current study attempted to collect a larger number of test series, to generate a solid base for deriving the resistance per detail. Substantial differences in resistance are observed between many individual series. This results in large values of s if the data of all series per detail are pooled. Explanations for these differences are sought and subsets of data are considered with restricted geometries and load conditions relevant for OBD in practice. Design recommendations are derived from the data.

3. Results: Fatigue resistance per detail

3.1. Deck plate crack from the toe of the rib weld (Detail C1a)

Fig. 3 presents the available test data for detail type C1a using the hot-spot stress σ_{hs}. The figure also gives the Basquin relation (average with dotted curve, 95% confidence with solid curve). The specimens in the different series are composed of deck plate thickness ranging between 12 mm $\leq t_d \leq$ 16 mm, a rib web thickness of $t_s = 6$ or 8 mm, and a weld ranging from fillet [33] to a penetration ratio of $p = 0.8$ [34] (p defined in Fig. 2(a)) or melt through [35]. Most of the series are carried out on specimens that consist of a deck plate and a single rib, where the specimen has a limited width, but [21,36] used full-scale bridge decks. The hot-spot stress is generally based on measured strains, but in Yuan and Ocel [33,35] it is based on finite element calculation. The latter tests are of particular interest because various potential influencing parameters such as weld geometry have been varied in these tests. It follows that welds with small size have a relatively low fatigue resistance for Detail C1a, possibly related to the difficulty of creating smooth geometric transition at the weld toe in small size welds. A distinct effect of penetration is not present for Detail C1a, Fig. 4(a). The same conclusion based on a single series is made in [36].

All tests in Fig. 3 are carried out with the deck plate in bending with a stress ratio $R = \sigma_{min}/\sigma_{max} = 10$ [39], $R = -1$ [34,38], $R = -0.66$ [37], $R = 0$ [40] (with one test at $R = \infty$) and $R = 0.3$ [23,41]. The data demonstrate an effect of the stress ratio on the average fatigue resistance at 2 million cycles $\Delta\sigma_{2e6}$, Fig. 4(b). The mean stress at the decisive locations in an actual bridge deck is below 0 [21,42]. Therefore, a subset of the data is considered with the mean stress below zero ($R \leq -1$ and $R > 1$) and with nominal penetration ratios $0.7 < p < 0.85$. Fig. 3(b) shows this subset. The standard deviation of C (or, equivalently, the standard deviation of $\log_{10}(N)$), s, is lower and the fatigue reference resistance is higher for the subset compared to the entire database, see the first rows of Table 1.

Considering a subset of deck plates with $t_d = 10$ or 12 mm only, Fig. 3(c), $\Delta\sigma_C$ increases and s reduces further, see Table 1. Indeed, plate thickness is relatively important for weld toe cracks in plates loaded in bending [43] but most series used a thickness of 12 mm $\leq t_d \leq$ 16 mm. The FM model of Appendix is adopted to estimate the fatigue resistance for thick deck plates. The fatigue resistance predicted with the FM model for $t_d = 12$ mm deviates only 1% from the resistance of Fig. 3(c), giving confidence in the model. Applying the model to a 20 mm thick deck plate gives $\Delta\sigma_C = 143$ MPa.

3.2. Deck plate crack from the root of the rib weld (Detail C1b)

Fig. 5(a) presents the test data of Detail C1b. (Tests in [44] are excluded because the deck plate was loaded in tension instead of bending.) A large scatter is present between test series, see Table 1. This is attributed to the differences in test conditions and stress definition, see Table 2. To account for the difference in stress definition, the stress range of the full bridge and the full rib tests [26,36,45] in Fig. 5 is determined as 1.11/1.04 times the reported stress, with 1.04 being the

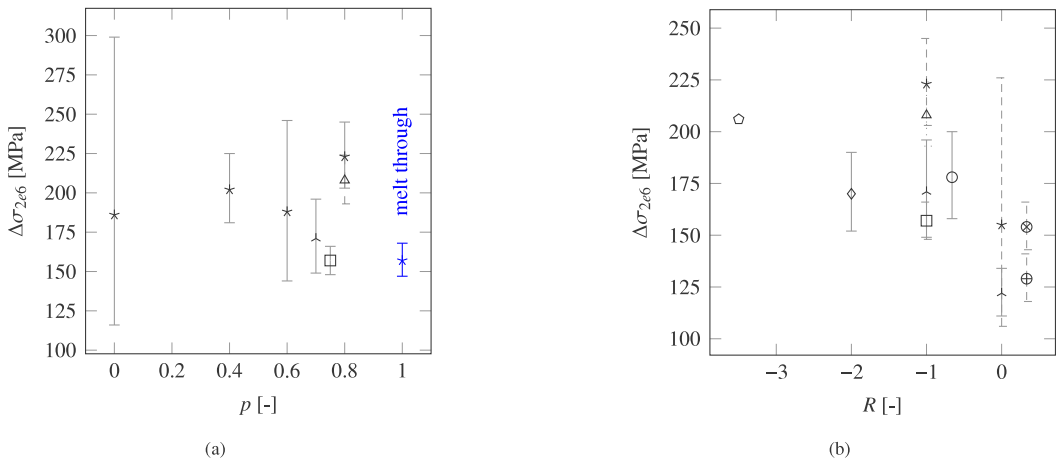

Fig. 4. Influence factors for Detail C1a, with point estimates (see Fig. 3 for symbol definitions) and 50% confidence interval (bars): (a) Effect of penetration ratio p on the mean fatigue resistance $\Delta\sigma_{2e6}$ at $R = -1$; (b) Effect of stress ratio R on the mean fatigue resistance of welds with $0.7 \geq p \geq 0.85$.

Table 1
Fatigue reference resistance $\Delta\sigma_C$ and standard deviation of $log_{10}(N)$, s, according to the Basquin fit of the number of n_f failed data out of the total number of n_t test data.

Detail	Subset	n_t	n_f	$\Delta\sigma_C$ [MPa]	s
C1a	All data	186	175	111	0.32
	$p > 0.7 \& R < 0$	53	50	153	0.21
	$p > 0.7 \& R < 0 \& t_d = 12$ mm	25	23	179	0.13
C1b	All data	122	98	81	0.36
	$h_1 = 0 \& R < 0$	30	19	130	0.26
	$h_1 = 2$ mm	38	38	78	0.24
C1c	$t_d = 10$ or 12 mm	47	34	162	0.27
	$t_d = 10$ or 12 mm, small load patch surface	18	7	277	0.09
	$t_d = 10$ or 12 mm, large load patch surface	32	27	167	0.18
C2a	All data	55	30	157	0.32
	Automatic weld & $p \geq 0.75$	24	9	275	0.10
	Manual weld & $p \geq 0.75$	10	9	159	0.14
C2b	All data	94	63	128	0.40
	Automatic weld & $p \geq 0.75$	54	34	158	0.30
	Manual weld & $p \geq 0.75$	10	8	105	0.22
	Manual fillet weld	37	27	97	0.22
C5	All data	77	68	101	0.30
	$R < 0 (R = -4)$	21	21	132	0.21
C6a	All data ($t = 6.4$ mm in bending)	9	9	154	0.15
C6b	All data	83	80	42	0.19
	S1 & $R \leq -1$	21	21	46	0.21
	S2 & $R \leq -1$	18	18	48	0.13
C7	All data (bending)	32	30	121	0.22

ratio of the stress 5 mm from the toe and the stress 5 mm from the root, and 1.11 being the ratio between the hot-spot stress and the stress 5 mm away from the root based on beam theory for the deck plate and checked with measured strain values in [26]. The nominal stress of the single rib web to deck plate specimens is not corrected because the stress concentration factor is expected to be close to 1.

None of the test series reported for Detail C1a contained cracks of type C1b, except for [36]. Sim and Uang [21] show that the effective notch stress at the weld root is approximately 15% lower as compared to the weld toe for welds with $p \approx 0.8$, irrespective of the lateral load position and deck plate thickness (ranging 12 mm $\leq t_d \leq$ 24 mm). Based on full-scale OBD tests, [52] concludes that cracks in Detail C1a are dominant for the loading pattern applied. Both C1a and C1b cracks are observed in [3,36,46,49], whereas only C1a cracks are observed in [23,34,37–41] and only C1b cracks are observed in [45,53,54] (reference to the latter two papers in [47]). An important influence factor is the load location: centred above or between ribs gives Detail C1a cracks and centred above the rib web gives predominantly C1b cracks in the full-scale tests of [36,45]. In the latter case, the hot-spot stress at the root and the toe side (i.e., inside and outside the rib) is approximately equal for the two details [45]. This implies that the fatigue resistance of Detail C1b should be similar to that of Detail C1a. The test results of [3,26,36,46] are in line with this but some of the other, especially plate to plate welded tests give a significantly lower resistance for Detail C1b.

A likely reason for the large scatter of test results for Detail C1b is the contact condition of the rib edge to the deck plate. If the rib is pressed against the deck plate during welding such that the lack of fit $h_1 = 0$ (Fig. 2(a)) weld shrinkage causes contact between the rib web edge and the deck plate [35] (Item 4 in Fig. 2(b)). Consequently, part of the load range is transferred through this contact point, thereby shielding the weld root location, giving a relatively high fatigue resistance. This implies that the weld geometry (related to the specimen preparation) and the stress ratio are extremely important for this detail. This also follows from the tests:

- The series carried out with a lack of fit ($h_1 = 2$ mm), likely to result in absence of contact, give the lowest fatigue resistance of the entire database, Fig. 5(b). These tests are relevant for the case that contact cannot be guaranteed.

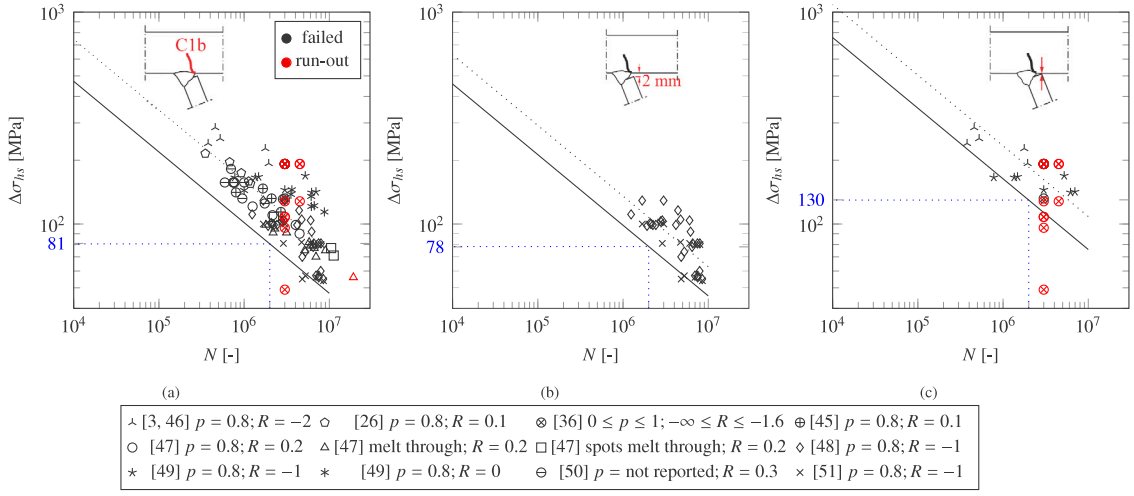

Fig. 5. Fatigue of Detail C1b, sources [3,26,36,45–51]: (a) All data; (b) Selection without contact between rib edge and deck plate; (c) Selection with contact.

Table 2
Test conditions of series for Detail C1b, sources [3,26,36,45–51].

Aspect	Description per series
Specimen geometry	Full decks with multiple ribs [36,45]. Single rib to deck plate [26]. Small specimens with one rib web cut from a rib to deck plate assembly [3,46,47,49,50]. Inclined plate single sided welded to another plate [48,51].
Weld geometry	Some tests in [47] with melt through, all other tests with $p \approx 1$. Lack of fit $h_1 = 2$ mm (see Fig. 2(a) for the definition), all other tests without (intentional) lack of fit.
Stress ratio	0.3 [50]; 0.2 [47]; 0.1 [26,45]; 0 [49]; −1 [48,49,51]; ≤ -1.7 [3,36,46].
Failure definition	Full-scale tests [36,45] terminated at a crack height of 3 to 8 mm. Other tests terminated at specimen failure or visually observed crack.
Stress definition	Hot-spot stress determined from measured strains [26,47]. Computed stresses from through-thickness linearisation in [18] for the data in [50]. Nominal stress (with unclear definition) [48]. Measured strain converted to nominal stress [3,46]. Measured strain converted to nominal stress near the toe side [36,45,51].

- The tests in [36] demonstrate a large influence of the stress ratio: Cracks are observed in tests with stress range $\Delta\sigma = 124$ MPa and mean stress $\overline{\sigma} = -16$ MPa whereas cracks are not observed in tests with $\Delta\sigma = 180$ MPa and $\overline{\sigma} = -90$ MPa (all test terminated at $N = 2 \cdot 10^6$).
- The tests without a lack of fit and with $\overline{\sigma} < 0$ ($R \le -1$) give the highest fatigue resistance of the entire database, Fig. 5(c).
- The tests in [47,52] indicate that melt-through may be (slightly) detrimental and should be avoided.

The tests in [26,45,47,50] are carried out in full tension ($R > 0$) and the contact point may then not be maintained during the entire load cycle. The fatigue resistance following from these tests is in between those of Fig. 5(b) and (c). As indicated before, $R > 0$ is not representative for the actual condition in OBD. It should be mentioned that the hot-spot stress definition according to Fig. 2(b) does not consider the effect of contact, because it is impractical to account for it. The effect is therefore implicitly considered in the fatigue resistance.

Double sided welds are proposed in [31,55,56] to improve the fatigue performance (i.e., get rid of) Detail C2b. It may be difficult to apply such a weld at deck splices to join large parts on site. Tests in [19,44,57] shows no or only a small benefit of double sided welds. Rolled ribs with thicker web edges are studied in [23] in an attempt to increase the fatigue resistance. They give a higher fatigue resistance compared to straight cold formed ribs for Detail C1a. However, the tests are carried out at a too high stress ratio for practice and Luo et al. [45] conclude that thick edge webs do not perform better for Detail C2b.

3.3. Deck plate crack from the root of the rib weld at the crossbeam (Detail C1c)

The difference between Detail C1b and Detail C1c is that the latter detail is located above a crossbeam, Fig. 6(a). The presence of the crossbeam causes a significant stress concentration at the hot spot. The detail is sensitive to crack initiation but, at reaching a depth of $a \approx 0.8t_d$, the crack propagates slowly, as demonstrated in tests with a fixed load position [58–60] or a moving wheel load [61], see Fig. 6(b). Slow crack propagation or crack arrest in thickness direction is attributed to the external load causing compression at the hot spot in combination with the decaying residual welding stress deeper into the plate. The decaying stress with increasing distance from the crossbeam, Fig. 6(c), is expected to be the main cause of slow crack propagation in length direction of the crack.

Fatigue tests for Detail C1c are reported using full-scale or component specimens with a 10 mm thick deck plate in [62], a 12 mm thick deck plate in [14,22,58–61,63] and a 16 mm thick deck plate in [59,64]. All test campaigns used a crossbeam thickness of 12 mm and a rib thickness of 6 or 8 mm. It is unknown if the contact point as described for Detail C1b is maintained after welding of the crossbeam web, but a comparison between welds with $p = 0.75$ and with controlled weld melt through in [22] demonstrates no significant influence of the root condition on the fatigue performance (although based on a limited number of tests). The failure criterion used for evaluating the data is a through-thickness crack that is visually detected from the top side of the deck plate. The tests in [61] and the 16 mm deck plate tests in [59] were terminated before the occurrence of a surface breaking crack and these are excluded here. The data in [64] are excluded because of a lacking definition of the reported stress.

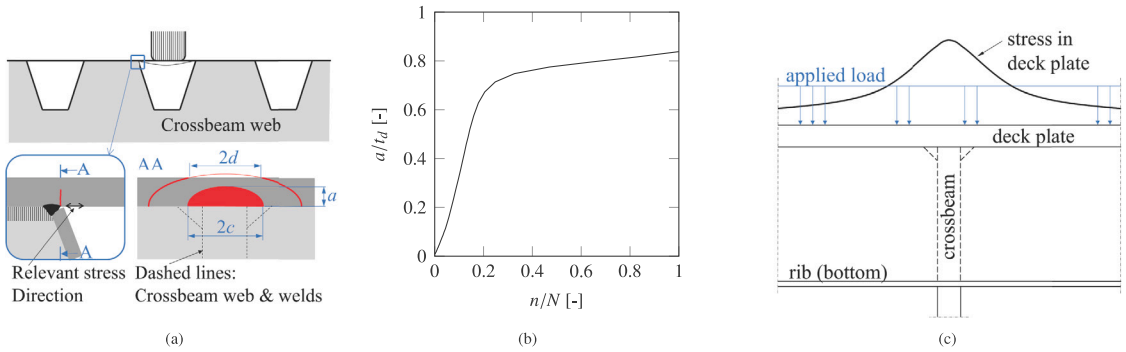

Fig. 6. Description of Detail C1c: (a) Geometry; (b) Schematic of crack propagation in depth (a) direction, based on [58–60]; (c) Stress decaying with distance from the crossbeam.

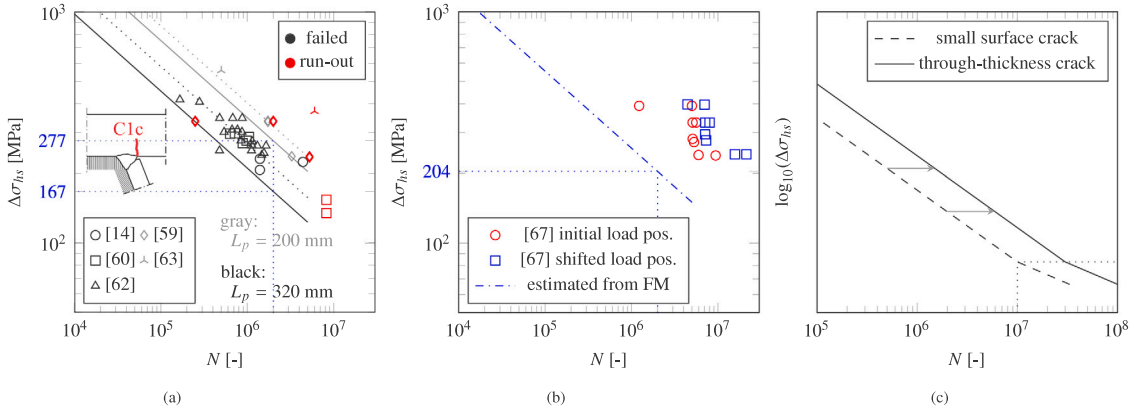

Fig. 7. Fatigue of Detail C1c, sources [14,58–60,62,63,67]: (a) Data with t_d = 10 and 12 mm (L_p = patch length); (b) Data and FM with t_d = 20 mm of current study (run-outs only); (c) Curve extension for VA load estimated from FM.

The FEM is employed to determine the hot-spot stress ranges in the tests. The model is validated with measured strains in [65]. Fig. 7(a) presents the test data for t_d = 10 or 12 mm, again showing significant scatter. The fatigue tests in [58,59,63] (displayed in grey) give a higher resistance than those in [14,60,62]. A possible reason for the difference is the load patch surface, which is longer and wider in the latter group (320 x 270 mm^2) compared to [58,59] (200 x 260 mm^2) and [63] (200 x 200 mm^2). As a result, the stress along the weld decays faster with distance to crossbeam (Fig. 6(c)) in [58,59,63] compared to [14,60,62]. The patch surface in the latter group is taken from Fatigue Load Model 4 in EN 1991-2 [6]. This surface appears too long for representing real traffic loads [66], however, a moving wheel creates a more uniform maximum stress along the weld compared to tests with a fixed load position [65], and the patch length of [14,60,62] is better aligned with this. Table 1 gives the statistical evaluation using all data and using the two groups. The high fatigue reference of $\Delta\sigma$ = 167 MPa is confirmed with FM simulations in [65] and it is related to the already mentioned decaying stress with distance to the crossbeam and the loading mode, causing plate bending with compression at the initiation point.

Because the tests available from literature are carried out with relatively thin decks, additional tests have been carried out by the authors with a thicker deck (t_d = 20 mm). Full details of the test set-up, the specimens and the results are given in the background report [67], a short description is given here. The specimen comprises of a deck plate supported by eight trapezoidal ribs and three crossbeams, with the bottom flange fully supported in vertical direction. Fig. 8(a) gives the rib dimensions. The fluctuating load (R = 0.1) is applied on a 180 x 320 mm^2 rubber patch, initially applied with its centre at the junction between the crossbeam and the rib centre of several ribs, Fig. 8(b). Cracks initiated almost from the start of testing and they grew in length direction at all tested locations, but they were not yet back-surface breaking at test termination ($10^6 \leq N \leq 10^7$). Because tyre loads cross an entire bridge deck in practice, the tests were continued with the load shifted 100 mm so that the applied load remained close to one of the crack edges, Fig. 8(c). The cracks grew further in length direction but only one surface breaking crack was obtained. The other test data, summarised in Fig. 7(b), are therefore considered as run-outs.

The fatigue resistance of Detail C1c with thick deck plates is further based on a FM model that is validated with the 12 mm deck plate test data, see [65]. This model uses the stress intensity factors for a rolling wheel obtained from the FEM. The model applied to t_d = 20 mm gives $\Delta\sigma_C$ = 204 MPa, with the corresponding curve added to Fig. 7(b). Both tests and FM show that the fatigue resistance *increases* for increasing deck thickness, with the loading mode changing from bending to punching. The FM based resistance for thick decks is lower than that of the tests. This is attributed to the use of a Paris equation constant for high stress ratios in the FM, thereby assuming high residual tensile stresses over the entire deck thickness. In reality, residual stress gradients and relaxation under loading may occur. Therefore, crack arrest may occur in reality, but this is not modelled with FM.

According to the FM simulations, the shape of the S–N curve deviates from that of ordinary details, namely, the knee point of the curve where the slope changes from m = −3 to m = −5 occurs at a much lower stress range as compared to that of usual details. A knee point of 54 MPa is calculated for both t_d = 12 and 20 mm. The low knee point is related to the quick initiation but slow propagation of the crack. This implies that the S–N curve shifts with respect to the number of cycles as compared to usual S–N curves as demonstrated in Fig. 7(c). Due to the conservative assumption for the crack growth rate as explained above, the S–N curve shape estimate may be conservative.

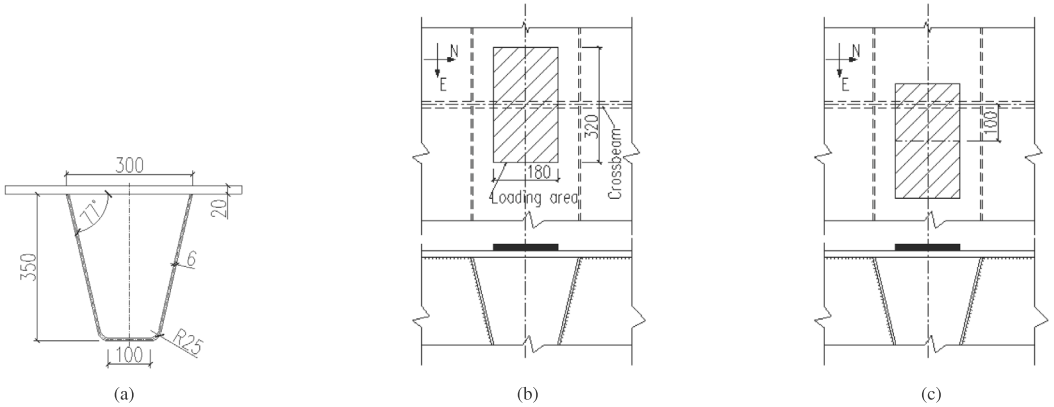

Fig. 8. Specimens of current study for Detail C1c (dimensions in mm, steel grade S355): (a) Rib and deck dimensions, crossbeam thickness = 16 mm; (b) Initial load position; (c) Shifted load position.

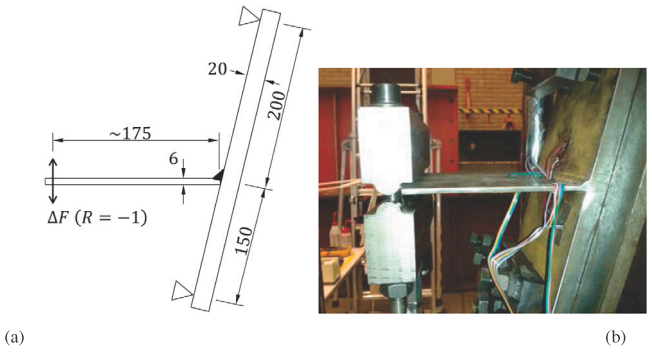

Fig. 9. Specimens of current study for Detail C2a and C2b, steel grade S355: (a) Dimensions (in mm); width = 200 mm; (b) Mounted in set-up.

3.4. Rib crack from the toe of the rib to deck weld (Detail C2a)

The worst load condition – giving the largest stress cycles – at the rib weld toe of the rib to deck weld is when wheels of trucks cross the bridge in alternating pattern either side of the rib web. The effective notch stress ratio is then $R \approx -1$ [21]. Tests with cracks in the rib web originating from the toe of the weld between the rib and the deck plate and with $R = -1$ are available from [33,68]. Tests are also reported in [44] but the hot-spot stress is not reported and the stress ratio $R = 0.1$ is too high for practice. These data are therefore excluded. Because of the limited number of available tests, additional tests have been carried out by the authors with two-pass automatic welds or one-pass manual overhead welds. The latter welding procedure is applied (in shop or on site) in assembling larger OBD parts. The test specimens and the set-up are similar to that in [68], see Fig. 9, and they are described in full detail in background report [69].

Cracks initiated in the weld toe and/or in the weld root in all test series. Tests with weld root cracks only are considered as run-outs. Fig. 10(a) gives all test data, with a distinction in colours between automatic welds with $p \geq 0.75$ (black), manual welds with $p \geq 0.75$ (grey) and welds with $p < 0.75$ (light grey). The figure demonstrates a clear distinction in fatigue resistance between automatic versus manual welds and large versus small penetration ratio. The difference between automatic and manual welds is attributed to the smoother weld toe transitions of the automatic welds (compare Fig. 10(b) and (c)). In order to study the influence of root penetration on the fatigue performance of the weld toe, the ENM is applied using the FEM for different penetration ratios. A model is made in the software Abaqus 2022 consisting of eight node plane strain elements with reduced integration, type CPE8R. The notch radii applied at the toe and at the root is 0.05 mm. Contact between the plates (Item 4 in Fig. 2(b)) is not modelled. The results are evaluated as the ratio between the maximum principal stress at the weld toe for $p = 1$ and for $p < 1$. This ratio corresponds well with the relative fatigue resistance as a function of p according to the tests in [33], see Fig. 10(d). It demonstrates the importance of the penetration ratio for Detail C2a.

The fatigue reference resistance is $\Delta\sigma_C = 275$ MPa for the automatic weld data with $p \geq 0.75$. This high fatigue resistance is attributed to the small plate thickness [32], the favourable stress condition (bending with $R = -1$) and the smooth weld toe transition. The fatigue reference resistance of manual welds with $p \geq 0.75$ is $\Delta\sigma_C = 159$ MPa and that of automatic welds with $p \approx 0.5$ is 123 MPa. Manual overhead welds possibly also give a worse performance than automatic welds for Detail C1a [70], but tests are lacking to confirm this.

3.5. Weld root crack in the rib to deck weld (Detail C2b)

Eq. (3) is proposed for evaluating the stress in the weld of Detail C2b. To verify this equation, the dependency of the stress on the penetration ratio is compared with the ENM (using the same model as discussed before, but now taking the maximum principal stress at the root). The good agreement between the two methods, Fig. 11, gives confidence in the appropriateness of Eq. (3).

Test data for automatic full or partial penetration welds ($p \geq 0.75$) are available from [33,68,71] and from the authors' own tests [69]. Test data for manual partial penetration welds are available from [72,73] and from the authors' own tests [69]. Tests with weld toe cracks only are considered as run-outs. The stress ranges are based on the average weld throat sizes and penetration ratios as reported (literature data) or obtained from the fracture surface [69]. The FEM is employed to evaluate the forces and bending moments in the rib webs, see Fig. 12 for an example of the tests with concentrated loads in [71].

Fig. 13(a) gives all fatigue test data, consisting of automatic welds with $p \geq 0.75$ (black), manual welds with $p \geq 0.75$ (grey), and welds with $p < 0.75$ (light grey). Most tests are carried out with $R \approx -1$, which is the relevant ratio for practice. The few data carried out at $R = 0$ are conservatively pooled with the other data. The scatter in the fatigue resistance is large, $s = 0.40$. This may be related to differences in the contact between rib edge and deck as discussed before and to irregularities of the root profile, the latter expected to be larger in manual as compared to automatic welds. The test series of Thonnard and Janss [72,73] has an exceptionally large scatter ($s = 0.48$) without clear correlation to the stress ratio or the penetration ratio. The measured strains reported in these tests deviate from the strains computed with the FEM model of Fig. 12, with inconsistent differences between individual tests. (This comparison is the reason for the dense mesh applied – a coarse mesh without explicit modelling of

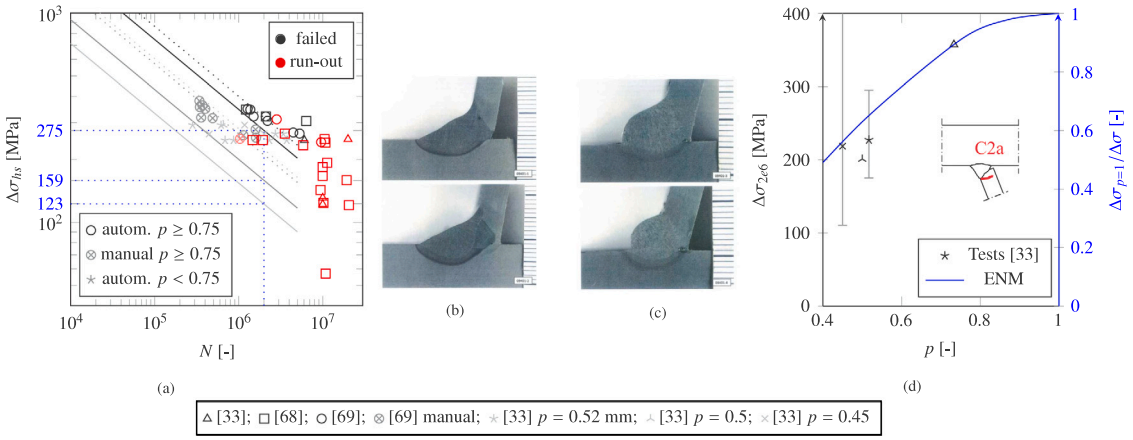

Fig. 10. Fatigue of Detail C2a at $R = -1$, sources [33,68,69]: (a) Test data; (b) Automatic weld cross-section photo; (c) Manual overhead weld cross-section photo; (d) Average fatigue resistance as a function of penetration ratio, according to the test data in [33] (black) with 50% confidence bound (grey) and relative according to the effective notch stress method (blue).

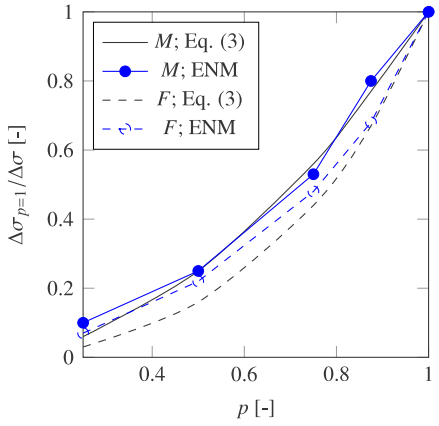

Fig. 11. Stress of Detail C2b for various penetration ratios p, relative to the stress at $p = 1$, according to Eq. (3) (black) and the effective notch stress method (ENM, blue) for a bending moment M (solid) and for a normal force F (dashed).

the lack of penetration is sufficient for the computation of the force and bending moment as input for Eq. (3).) The authors' test results with manual welds [69] are at the lower bound of the test results of [72,73]. For these reasons, the data of [72,73] are excluded from the evaluation. Fig. 13(b) and (c) provide subsets of the database for automatic and manual welds, respectively. The resulting fatigue reference resistances are $\Delta\sigma_C = 158$ and 105 MPa, respectively.

Because the fatigue reference resistance of the manual partial penetration welds is based on one series only, test data of manual fillet welds are also collected and evaluated, Fig. 13(d). The weld stress according to Eq. (3) is determined from the reported membrane and bending stress, weld throat size and penetration ratio. The resulting fatigue reference resistance $\Delta\sigma_C = 97$ MPa is close to that of the manual partial penetration welds, giving support of the resistance of the latter subset. Note that the effect of penetration is considered in the stress for this detail, Eq. (3). Fig. 11 indicates that fillet welds give a significantly higher weld stress than welds with $p = 0.8$. A lower fatigue performance of fillet welds is also observed in [20]. The data for fillet welds are therefore included for reference, but not recommended for practical use.

3.6. Crack in the deck from the toe of the crossbeam-to-deck weld (Detail C5)

Wheels crossing a bridge induce bending in the deck plate with predominantly compression at the weld with the crossbeam. OBD tests with weld toe cracks at this location have not been found [74]. Fig. 14(a) provides test data from small-scale tests with a main plate loaded in bending to which a single sided attachment is welded with cracks at the weld toe in the main plate. The main (deck) plate thickness, attachment (crossbeam) thickness and weld throat ranged between 9 mm $\leq t_d \leq$ 24 mm, 6 mm $\leq t_c \leq$ 16 mm and 4 mm $\leq a_w \leq$ 6 mm, respectively. Some series are evaluated with the nominal stress method and others with the hot-spot stress method. The data are pooled because the hot-spot stress range is almost equal to the nominal stress range in these specimens [75]. The relatively large scatter of the test data – $s = 0.3$ – is attributed to differences in plate thickness and stress ratio. As the weld toe is loaded predominantly in compression in the practical situation, Fig. 14(b) gives a subset specimens in bending with $R < -1$ at the initiation site, resulting in a reduced standard deviation

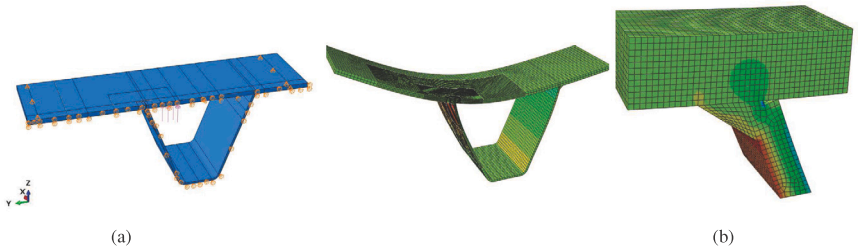

Fig. 12. Finite element model in Abaqus 2022 using quadratic (20-node) solid elements with reduced integration of Type C3D20R, size $1 \times 1 \times 1$ mm^3 in the area of interest, for evaluating the tests in [71–73]: (a) Geometry, load and boundary conditions; (b) deformed mesh with contour plot of stress aligned with rib web (red colour = high stress).

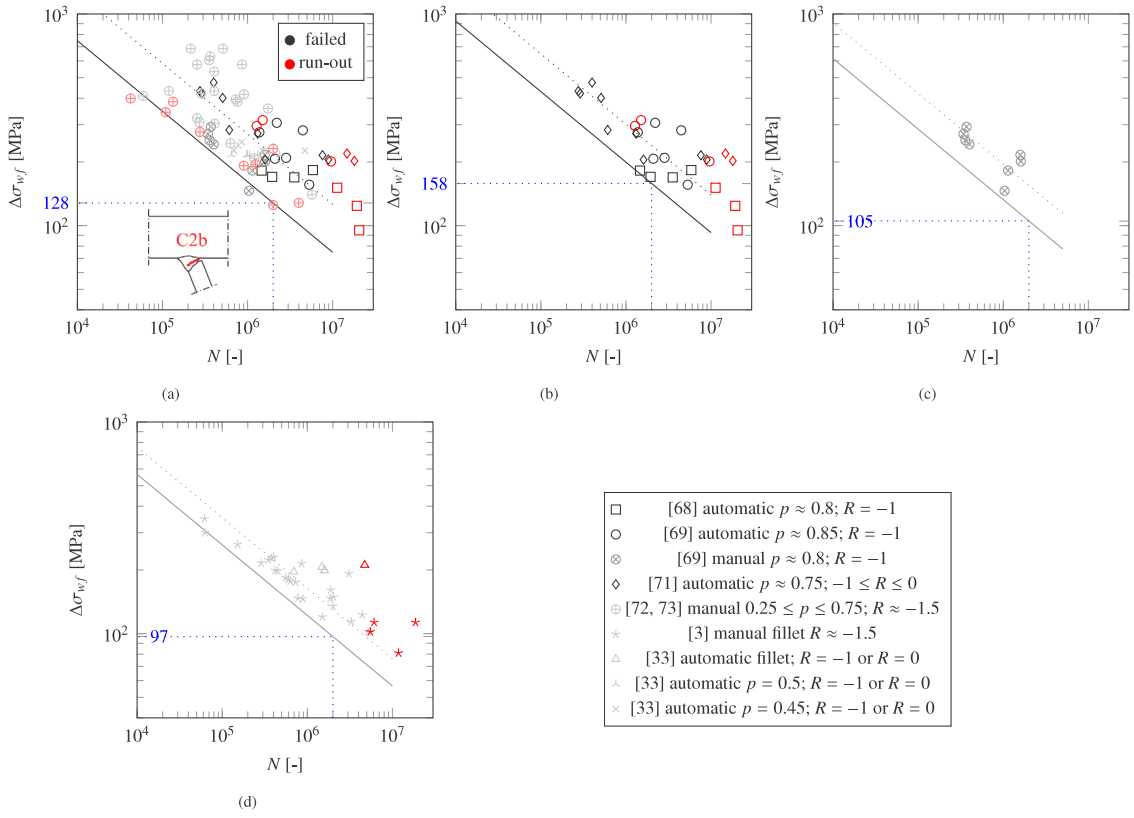

Fig. 13. Fatigue of Detail C2b, sources [3,33,68,69,69,71–73]: (a) Partial penetration welds; (b) Automatic partial penetration welds; (c) Manual partial penetration welds excluding [72,73]; (d) Manual fillet welds.

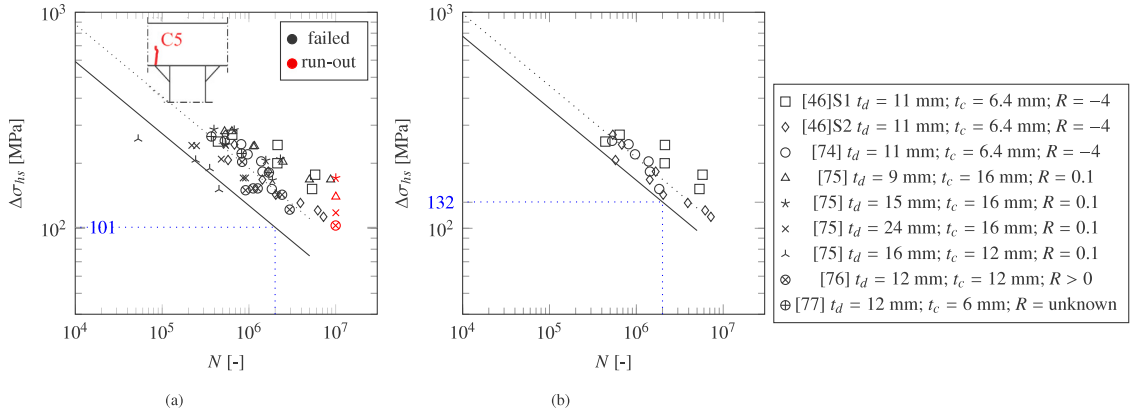

Fig. 14. Fatigue of Detail C5, sources [46,74–77]: (a) All data; (b) Tests with $R < -1$ ($R = -4$).

and an increased fatigue reference resistance, see Table 1. However, the subset contains thin plates only. Simulations with FM (Appendix) with the same dimensions as in the test give almost the same fatigue resistance ($\Delta\sigma_C = 129$ MPa). The same model employed to ($t_d = 12$ mm; $t_c = 12$ mm) and to ($t_d = 20$ mm; $t_c = 20$ mm) gives a reduction in the fatigue resistance of 2% and 13%, respectively.

3.7. Crack in the crossbeam from the toe of the crossbeam-to-deck weld (Detail C6a)

Wheels crossing a bridge induce a combination of bending and compression in the crossbeam web near the weld with the deck plate. Cracks are not observed at this location in bridge deck tests in [74,78] despite of the high stress ranges applied. Fig. 15 presents the results of a limited number of small-scale tests with relatively thin loaded (crossbeam) plates ($t = 6.4$ mm), carried out at $R = \infty$. Weld root failures are not observed in these tests even though fillet welds are applied. This may be caused by the excessive weld throat dimensions used in these tests ($a_w = 6$ or 9 mm).

The number of tests found is limited and the rib thickness is too small to represent real crossbeams. Cruciform joints with the interrupted plate loaded in tension or bending are widespread, but these may not be representative for this detail because of the different stress path and the potential influence of misalignment in cruciform joints.

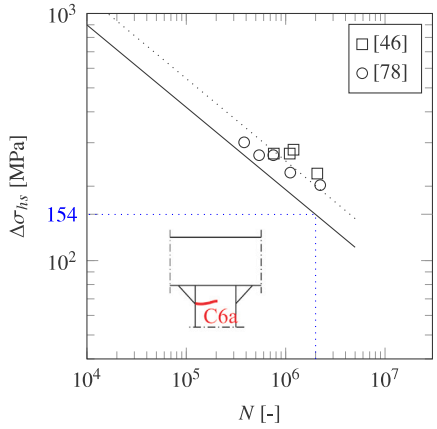

Fig. 15. Fatigue of Detail C6a, sources [46,78].

FM is employed for this reason, giving the same fatigue resistance as the test ($\Delta\sigma_C$ = 154 MPa) for the same dimensions and a fatigue resistance reduction of 18% and 27% for (t_d = 12 mm; t_c = 12 mm) and (t_d = 20 mm; t_c = 20 mm), respectively, in case of full penetration welds ($\Delta\sigma_C$ = 126 MPa and $\Delta\sigma_C$ = 112 MPa, respectively). For toe cracks at fillet welds, EN 1993-1-9 [7] provides a hot-spot stress fatigue resistance equal to 90% of that of full penetration welds. Using the same fraction, the fatigue reference resistance of the toe crack in case of fillet welds is estimated as $\Delta\sigma_C = 112 \cdot 0.90 = 100$ MPa.

3.8. Crack in the weld from the root of the crossbeam-to-deck weld (Detail C6b)

None of the tests on crossbeam to deck welds (previous subsections) showed cracks in the weld. The fatigue reference resistance in case of weld root failure in cruciform joints is determined as $\Delta\sigma_C$ = 38 MPa in [28]. The scatter of the test data collected in [79] reduces significantly if a subset with high maximum stress is considered. The detail in OBD is loaded predominantly in compression. This may result in an increased fatigue resistance particularly if the deck plate and crossbeam are in full contact at the unfused land. Test data with weld root failure in [10] carried out at R = −1 give $\Delta\sigma_C$ = 58 MPa and a large scatter. Additional tests on cruciform joints have been carried out by the authors to further examine the effect of weld root failure for different stress ratios, with a full description in background report [80].

Two series are conducted, series S1 is welded with a usual procedure and series S2 is welded with an intended lack of fit between the plates, see Fig. 16(a). The plates are of steel grade S355 and all welds are manually welded with a Tenax CY17 electrode. The tests – 80 in total – were carried out at stress ratios R = −2, −1, 0 and 0.5. Fig. 16(b) gives the test results. A significant influence of the stress ratio is observed for Series S1, but only at a relatively high stress range. The stress ratio effect is not significant in Series S2. This is further demonstrated in Fig. 16(c), where the average fatigue resistance $\Delta\sigma_{2e6}$ is estimated from Eq. (4) at each test condition with applied stress range and stress ratio. Even though the geometry of Detail C6b is different from that of a cruciform joint, the figure indicates that one should be careful with relying on a large mean stress effect for weld root cracks.

3.9. Crack from the deck butt joint (Detail C7)

In the vast majority of bridges, the deck plate is loaded almost exclusively in bending and this has a positive influence on the fatigue resistance of deck butt welds, [81]. An important aspect is that misalignments do not influence the fatigue resistance in bending. Full-scale tests with cracks in detail C7 have not been found. Double sided welds are usually applied except for the part of the transverse weld above the rib that is required to assemble large decks. However, the latter single sided (V-groove) weld is not heavily stressed and tests (in tension) in [82,83] showed cracks from the toe. Cracks from the root are therefore not considered here. Only two series with butt welded specimen in as welded condition loaded in bending are found, Fig. 17. The series are not well representative of OBD because the plate thickness of 30 mm in [84] is larger than the typical deck plate thickness and the tests of [85] are carried out during or after saline water exposure with R = 0.1. Both series are expected to be conservative for deck plates in OBD.

FM is employed to estimate the fatigue resistance of butt joints loaded in bending. The resulting fatigue reference resistance is $\Delta\sigma_C$ = 129 and 159 MPa for as-welded and ground flush welds, respectively, for t_d = 20 mm. These values are $\Delta\sigma_C$ = 141 and 162 MPa, respectively, for t_d = 12 mm.

4. Proposed FAT classes

The FAT class – called detail category in [7] – defines the fatigue resistance that can be used in the design. Following the convention of EN 1993-1-9 [7], the FAT class is obtained by rounding down the

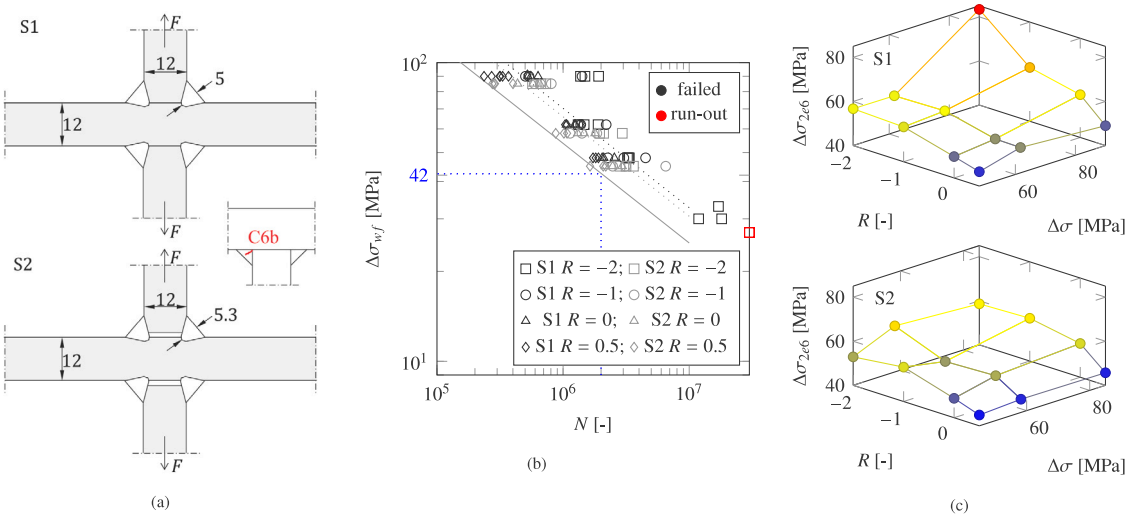

Fig. 16. Fatigue of Detail C6b (current study): (a) Specimens of Series S1 and S2 (dimensions in mm, specimen width = 120 mm); (b) Test data; (c) Influence of stress ratio and tested stress range on fatigue resistance estimate (S1 in top figure: S2 in bottom figure).

Table 3
Proposed FAT classes (implemented in TS 1993-1-901 [24]).

Detail	Stress	FAT	Condition	Source
C1a	σ_{hs} (Eq. (1))	140	$t_d \leq 14$ mm	Fig. 3(b–c)
		125	$t_d > 14$ mm	FM (Section 3.1)
C1b	σ_{hs} (Eq. (1))	125	$h_1 = 0$ mm	Fig. 5(c)
		80	$h_1 > 0$ mm	Fig. 5(b)
C1c	σ_{hs} (Eq. (1))	170	$t_d \leq 14$ mm	Fig. 5(a)
		190	14 mm $< t_d <$ 18 mm	Interpolated
		200	$t_d \geq 18$ mm	Fig. 5(b) and FM (Section 3.2)
C2a	σ_{hs} (Eq. (1))	160	–	Fig. 10(a) Manual and automatic welds combined because of small number of data
C2b	σ_{wf} (Eq. (3))	140	Automatic weld	Fig. 13(b)
		100	Manual weld	Fig. 13(c–d)
C5	σ_{hs} (Eq. (1))	125	$t_d \leq 14$ mm	Fig. 14(b) and FM (Section 3.6)
		112	$t_d > 14$ mm	FM (Section 3.6)
C6a	σ_{hs} (Eq. (1))	112	Full penetration weld	Fig. 15 and FM (Section 3.7)
		100	Fillet weld	FM and [8] (Section 3.7)
C6b	σ_{wf} (Eq. (2))	40	Fillet weld	[8]; Section 3.8
C7	σ_{hs} (Eq. (1))	140	Weld ground flush	FM (Section 3.9)
		125	Flank angle $\geq 150°$	Fig. 17 and FM (Section 3.9)

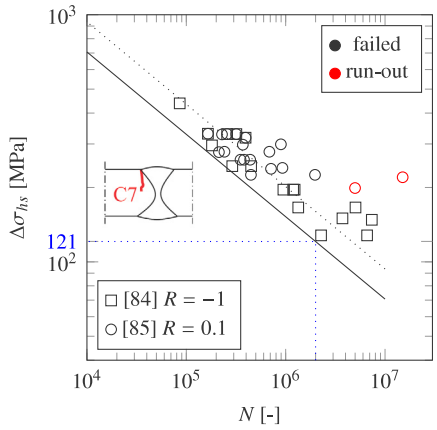

Fig. 17. Fatigue of Detail C7, sources [84,85].

fatigue reference resistance divided by MPa to one of the predefined classes. The lowest predefined FAT class is 36 and each subsequent class has an incremental increase of approximately 12.5%. The FAT classes of Table 3 are proposed based on the data in Section 3.

The FAT classes of Table 3 apply to loading modes and stress ratios relevant to OBD and they are implemented in TS 1993-1-901 [24]. They apply only to rib to deck welds with smooth weld toe transitions. Following [35] and the authors' tests, the weld should be extended with weld leg lengths in the order of the stiffener web thickness to accommodate this. Further, the welds should have a high penetration ratio ($p \approx 0.8$ or larger) but melt through should be prevented (relevant for Details C2a and C2b). This is put forward in TS 1993-1-901 [24] by specifying $h_4 = t_s \pm 1$ mm and $h_3 = t_s \pm 1$ mm. The practical condition given to ensure contact between the plates for Details C1b and C2b is $h_1 = 0$ mm over 90% of the weld length (achieved in practice by pressing the rib to the deck during welding). Table 1 shows that the subsets satisfying the conditions in Table 3 give standard deviations s close to the often-assumed value for welded joints of 0.2 [11]; a substantial reduction compared to the standard deviations of the complete databases per detail.

5. Conclusions

This paper estimates the fatigue resistance of various deck plate details in orthotropic bridge decks from tests and fracture mechanics simulations. The authors have carried out additional tests for details lacking data. The hot-spot stress method is applied, except for weld throat cracks. A simple equation (Eq. (3)) is proposed for weld root cracks in the single sided rib to deck weld. A comparison with the effective notch stress method indicates that this equation can capture the effect of loading mode and lack of penetration of the weld.

High fatigue resistances are obtained (Table 3), attributed to favourable loading modes (bending or compression for many details), cracks growing into regions of reduced crack driving force, and small plate thickness particularly for the rib. As a result, the crack growth rate is typically low compared to simple welded details loaded in tension. The geometry of particularly the rib to deck weld appears crucial for obtaining these high fatigue resistances. The weld toe transitions should be smooth, requiring the weld to be extended to the outer

Table A.4
Applied equations and parameters of the fracture mechanics model.

Parameter	Value or equation source
SIF semi-elliptical surface crack	Equations in [86,87]
SIF correction for weld toe	Equations in [88]
Weld flank angle	135° for cruciform joints and welded attachments, 150° for butt joints and 180° for ground flush butt joint (SIF equation in [89])
Weld toe radius	1 mm (SIF equation in [89])
Axial eccentricity between plates	5% of plate thickness for butt welds and cruciform welds 0% for welded attachments (SIF equation in [90])
Initial crack depth	$a = 0.15$ mm
Initial crack length	$2c = 0.30$ mm
Failure criterion	Surface breaking crack
Crack growth rate	Two-stage relation for $R \geq 0.5$ in air in [90]

side of the rib web. The lack of fit between rib and deck should be minimised to generate contact between these plates, thereby obtaining a high resistance against a deck plate crack from the weld root. The penetration ratio should be large (at least 80%) but melt through should be prevented for a high resistance against weld and rib web cracks. Manual overhead welds are shown to perform worse than automatic welds in flat position, probably due to less smooth weld toe transitions. Although the importance of some of these aspects has already been emphasised by others, their effects are now quantified by a sufficiently large number of tests from different series.

The standard deviations of the logarithm of the number of cycles to failure are large (often 0.3 or 0.4) if all date of one crack type are pooled. The standard deviations reduce to values conveniently close to the standard value of 0.2 if considering subsets of the data with similar geometry, loading mode and stress ratio, see Table 1. However, one should be careful in relying on a favourable effect of the negative stress ratio in root cracks of fillet welds between the crossbeam web and the deck, especially if a lack of fit may apply (which is almost unavoidable for this detail in practice).

A fatigue test program of deck plate cracks from the toes of manual overhead welds has not been found. Such welds are unavoidable for connecting large OBD parts on site. They have shown to perform worse for cracks in the weld and in the rib web. Such a test program would be welcome.

CRediT authorship contribution statement

Johan Maljaars: Conceptualization, Analysis, Writing, Data collection. **Richard Pijpers:** Data collection, Analysis. **Weijian Wu:** Finite element analysis, Data collection. **Henk Kolstein:** Data collection, Reviewing.

Declaration of competing interest

We wish to confirm that there are no known conflicts of interest associated with this publication and there has been no financial support for this work such, that it could have influenced its outcome.

Data availability

Data will be made available on request.

Acknowledgements

This study is sponsored by Rijkswaterstaat. The authors acknowledge Frank van Dooren and Bas Wijnbeld for their review of the FAT classes and Jorrit Rodenburg for employing the FEM for the stress estimates of [71–73], Fig. 12.

Appendix. Description and validation of the fracture mechanics model

This Appendix describes the linear elastic Fracture Mechanics (FM) model used to estimate the fatigue resistance of details in OBD with cracks growing from the weld toe. The model is validated using well established fatigue resistances for plates loaded in tension and using results of individual test series for plates loaded in bending.

FM theory is considered suited for evaluating the fatigue resistance of welded details since the life of welded details is dominated by crack propagation. The basis of the model employed here is the British standard BS 7910:2019 [90]. Standard equations for describing the Stress Intensity Factor (SIF) are considered valid for all weld toe details of study. Table A.4 provides the applied equations and parameters in the model. A dedicated model, with SIF values determined from the FEM, is used for Detail C1c, see [65] for the details and the validation. Specific attention is required for the assumption of the initial crack size. The value used here is a calibration value as derived and adopted by many others to evaluate the fatigue life of an as-welded detail using one single semi-elliptical crack.

The nominal fatigue reference resistance is calculated from the FM life predictions using the characteristic (5% exceedance) crack growth rate. For plates with a thickness of 25 mm and axial loading, the fatigue reference resistance values are 129 MPa, 94 MPa, 77 MPa and 69 MPa for ground flush butt joint, an as-welded butt joint, a welded attachment and a cruciform joint, respectively. The corresponding nominal fatigue reference resistance according to the standard EN 1993-1-9 [8] are 112 MPa, 90 MPa, 80 MPa and 71 MPa, respectively (similar values given in other standards or guidelines). The FM prediction agrees well with the standard [8] except for the ground flush butt joint detail. However, a collection of tests on the latter detail in [91] gives a fatigue reference strength of 127 MPa, indicating that the standard is conservative for this detail, and it is in a good agreement with the FM prediction.

Fig. A.18 gives a comparison of the fatigue resistance of different test series with plates loaded in bending and containing welded attachments (dots) and the FM prediction thereof using the average crack growth rate (curves). The different colours indicate different series (with specific geometry). The nominal stress is equal to the hot-spot stress in these simple geometries loaded in bending [75]. The average fatigue resistance ranges between 115 MPa $\leq \Delta\sigma_{2e6} \leq$ 202 MPa. The ratio between the predicted and the tested fatigue resistance is on average 1.0 and the standard deviation is 0.12. The decreasing resistance with increasing plate thickness and weld toe to weld toe distance agrees reasonable between FM and tests.

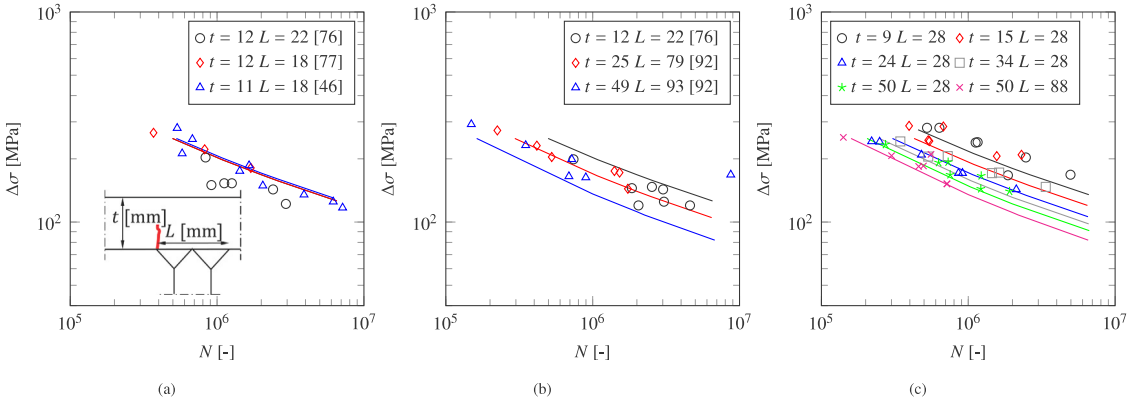

Fig. A.18. Fatigue tests of welded plates in bending (dots – only failed data displayed) and the prediction thereof using fracture mechanics (curves): (a) Welded attachments in [76] (with data from [46,77]); (b) Cruciform joints in [76] (with data from [92]); (c) Welded attachments in [75].

References

[1] Hänsch H, Müller G. Dauerfestigkeitsversuche an geschweissten Hohlrippenanschlüssen. Schweisstechnik 1961;11:193–8.
[2] Erzurumlu H, Topac AA. Fatigue of orthotropic steel decks. J Struct Div 1972;98:813–30.
[3] Maddox S. The fatigue behaviour of trapezoidal stiffener to deck plate welds in orthotropic bridge decks, supplementary report 96uc. Tech. rep., Transport and Road Research Laboratory; 1974.
[4] Chen J, Wei C, Zhao Y. Fatigue resistance of orthotropic steel deck system with double-side welded rib-to-deck joint. Adv Struct Eng 2022;1–14.
[5] Da L-T, Zhang Q-H, Yuan D-Y, Ma Y, Cui C. A new orthotropic steel deck system incorporating two novel structural details. J Constr Steel Res 2022;199:107633.
[6] EN 1991-2 + C1. Eurocode 1: actions on structure – part 2: traffic loads on bridges. CEN; 2015.
[7] EN 1993-1-9 + C2. Eurocode 3: design of steel structures – part 1-9: fatigue. CEN; 2009.
[8] prEN 1993-1-9. Eurocode 3: design of steel structures – part 1-9: fatigue. Doc N3751 (enquiry draft). CEN; 2023.
[9] AASHTO LRFD. Bridge design specifications. American association of state highway and transportation officials; 2012.
[10] Hobbacher A. Recommendations for fatigue design of welded joints and components. Springer; 2016.
[11] DNV-RP-C203. Fatigue design of offshore steel structures. DNV; 2021.
[12] BS 7608. Guide to fatigue design and assessment of steel products. BSI; 2014.
[13] Maljaars J, van Dooren F, Kolstein H. Fatigue assessment for deck plates in orthotropic bridge decks. Steel Constr 2012;5(2):93–100.
[14] Kolstein M. Fatigue classification of welded joints in orthotropic steel bridge decks [Ph.D. thesis], Delft University of Technology; 2007.
[15] Liu R, Liu Y, Ji B, Wang M, Tian Y. Hot spot stress analysis on rib–deck welded joint in orthotropic steel decks. J Constr Steel Res 2014;97:1–9.
[16] Wang B, Lu P, Shao Y. Research on rib-to-diaphragm welded connection by means of hot spot stress approach. Steel Composite Struct 2015;18:135–48.
[17] Yokozeki K, Tominagao T, Miki C. Experimental fatigue assessment of connections between plate-type longitudinal ribs and non-slit transverse ribs in orthotropic steel decks. Weld World 2021;65:623–33.
[18] Luo P, Zhang Q, Bao Y. Rib loading effects on weld root fatigue failure modes at rib-to-deck welded joint. Fatigue Fract Eng Mater Struct 2020;43:1399–418.
[19] Yang H, Wang P, Qian H, Dong P. Analysis of fatigue test conditions for reproducing weld toe cracking into U-rib wall in orthotropic bridge decks. Int J Fatigue 2022;162:106976.
[20] Li J, Zhang Q, Bao Y, Zhu J, Chen L, Bu Y. An equivalent structural stress-based fatigue evaluation framework for rib-to-deck welded joints in orthotropic steel deck. Eng Struct 2019;196:109304.
[21] Sim H-B, Uang C-M. Stress analyses and parametric study on full-scale fatigue tests of rib-to-deck welded joints in steel orthotropic decks. J Bridge Eng 2012;17:765–73.
[22] Dung C, Sasaki E, Tajima K, Suzuki T. Investigations on the effect of weld penetration on fatigue strength of rib-to-deck welded joints in orthotropic steel decks. Int J Steel Struct 2015;15:299–310.
[23] Heng J, Zheng K, Gou C, Zhang Y, Bao Y. Fatigue performance of rib-to-deck joints in orthotropic steel decks with thickened edge u-ribs. J Bridge Eng 2017;22:4017059.
[24] TS 1993-1-901. Fatigue design of orthotropic bridge decks with the hot spot stress method (final draft). CEN; 2023.
[25] Ahola A, Hamidreza RR, Björk T, Kukkonen O. On the interaction of axial and bending loads in the weld root fatigue strength assessment of load-carrying cruciform joints. Weld World 2022;66(4):731–44.
[26] Wang D, Xiang C, Ma Y, Chen A, Wang B. Experimental study on the root-deck fatigue crack on orthotropic steel decks. Mater Des 2021;203:109601.
[27] Drebenstedt K, Euler M. Statistical analysis of fatigue test data according to Eurocode 3. In: Proc. maintenance, safety, risk, management and life-cycle performance of bridges. CRC Press; 2018, p. 2244–51.
[28] Bartsch H, Drebenstedt K, Seyfried B, Feldmann M, Kuhlmann U, Ummenhofer T. Analysis of fatigue test data to reassess EN 1993-1-9 detail categories. Steel Constr 2020;13(4):280–93.
[29] Schneider CRA, Maddox SJ. Best practice guide on statistical analysis of fatigue data. TWI doc. 13604.01/02/1157.02. The Welding Institute; 2002.
[30] Hensel J, Nitschke-Pagel T, Dilger K. Engineering model for the quantitative consideration of residual stresses in fatigue design of welded components. Weld World 2017;61:997–1002.
[31] Liu Y, Chen F, Wang D, Lu N. Fatigue crack growth behavior of rib-to-deck double-sided welded joints of orthotropic steel decks. Adv Struct Eng 2021;24(3):556–69.
[32] Sonsino CM, Bruder T, Baumgartner J. S-N lines for welded thin joints - Suggested slopes and FAT values for applying the notch stress concept with various reference radii. Weld World 2010;54:R375–92.
[33] Yuan H. Optimization of rib-to-deck welds for steel orthotropic bridge decks. Tech. rep., Virginia Polytechnic Institute and State University; 2011.
[34] Li M, Suzuki Y, Hashimoto K, Sugiura K. Experimental study on fatigue resistance of rib-to-deck joint in orthotoropic steel bridge deck. J Bridge Eng 2018;23:4017128.
[35] Ocel J, Cross B, Wright W, Yuan H. Optimization of rib-to-deck welds for steel orthotropic bridge decks. Tech. rep., Federal Highway Administration – US Department of Transportation; 2017.
[36] Kainuma S, Yang M, Jeong Y-S, Inokuchi S, Kawabata A, Uchida D. Experimental investigation for structural parameter effects on fatigue behavior of rib-to-deck welded joints in orthotropic steel decks. Eng Fail Anal 2017;79:520–37.
[37] Dijkstra O, Nicolaas T. Fatigue study for repair method trough deck plate connection Moerdijk bridge, TNO 2000-CON-R4016 (in Dutch). Tech. rep., TNO; 2000.
[38] Bignonnet A, Jacob B, Caracilli J, LaFrance M. Fatigue resistance of orthotropic steel decks. In: Proc. IABSE workshop remaining fatigue life of steel structures. 1991, p. 227–36.
[39] Cheng B, Ye X, Cao X, Mbako D, Cao Y. Experimental study on fatigue resistance of rib-to-deck joint in orthotoropic steel bridge deck. Int J Fatigue 2017;103:157–67.
[40] Nagy W. Fatigue assessment of orthotropic steel decks based on fracture mechanics [Ph.D. thesis], Ghent University; 2017.
[41] Heng J, Zheng K, Feng X, Veljkovic M, Zhou Z. Machine learning-assisted probabilistic fatigue evaluation of rib-to-deck joints in orthotropic steel decks. Eng Struct 2022;265:114496.
[42] Xiao Z-G, Yamada K, Ya S, Zhao X-L. Stress analyses and fatigue evaluation of rib-to-deck joints in steel orthotropic decks. Int J Fatigue 2008;30(8):1387–97.
[43] Shen W, Qiu Y, Xu L, Liu E. A semi-analytical formula for calculating the notch stress field of cruciform welded joint under bending loading. Fatigue Fract Eng Mater Struct 2020;43:2637–52.
[44] Yang H, Wang P, Qian H, Niu S, Dong P. An experimental investigation into fatigue behaviors of single- and double-sided U rib welds in orthotropic bridge decks. Int J Fatigue 2022;159:106827.
[45] Luo P, Zhang Q, Bao Y, Bu Y. Fatigue performance of welded joint between thickened-edge U-rib and deck in orthotropic steel deck. Eng Struct 2019;181:699–710.
[46] Maddox S. Fatigue of welded joints loaded in bending (Report 84UC). Tech. rep., Transport and Road Research Laboratory; 1974.

[47] Ya S, Yamada K, Ishikawa T. Fatigue evaluation of rib-to-deck welded joints of orthotropic steel bridge deck. J Bridge Eng 2011;16(4):492–9.
[48] Fu Z, Hi B, Zhang C, Li D. Experimental study on the fatigue performance of roof and U-rib welds of orthotropic steel bridge decks. KSCE J Civil Eng 2018;22:270–8.
[49] Yamada K, Ya S. Plate bending fatigue tests for root crack of trough rib of orthotropic steel deck. Jap J Struct Eng 2008;54:675–84.
[50] Lv P, Li D. Fatigue test research of rib-to-deck welded joints of orthotropic steel deck. J Zhengzhou Univ Eng Sci 2013;34:89–93.
[51] Zhiyuan Y-Z, Bohai J, Di L, Zhongqiu F. Fatigue strength and root deck crack propagation for U rib to deck welded joint in steel box girder. Int J Steel Struct 2018;18(5):1589–97.
[52] Sim H-B, Uang C-M, Sikorsky C. Effects of fabrication procedures on fatigue resistance of welded joints in steel orthotropic decks. J Bridge Eng 2009;14:366–73.
[53] Mori T, Shigihara S, Nakamura H. Fatigue tests on welded connections between deck plate and trough rib in steel plate deck in consideration of weld penetration (in Japanese). Doboku Gakkai Ronbunshu A [J JSCE] 2006;62(3):570–81.
[54] Kawabata A, Inokuchi S, Hironaka O, Suzuki O, Saito S. Wheel trucking test for welding of U-shaped rib and deck plate of the orthotropic decks (in Japanese). In: Proc. 5th symposium of orthotropic steel bridge decks. 2006, p. (no page numbers).
[55] Fang Z, Ding Y, Wei X, Li A, Geng F. Fatigue failure and optimization of double-sided weld in orthotropic steel bridge decks. Eng Fail Anal 2020;116:104750.
[56] Zhu Z, Li J, Chen X, Carpinteri A. Stress behaviors of rib-to-deck double-sided weld detail on orthotropic steel deck. J Constr Steel Res 2021;187:106947.
[57] Nishida N, Sakano M, Tabata A, Sugiyama Y, Okumura M, Natsuki Y. Fatigue behavior of orthotropic steel deck with both side fillet welds between deck and trough ribs. In: Proc. 68th JSCE annual meeting. 2013, p. 4–6.
[58] Mori T, Uchida D. Propagation behavior of fatigue crack penetrating into steel deck plate at connection with transverse rib and trough rib - IIW doc. XIII-2433-12. Tech. rep., International Institute of Welding; 2012.
[59] Hayashi N, Kudo Y, Okumura M, Uchida D, Mori T. Influence of load range on fatigue crack propagation behaviour in orthotropic steel deck. In: Proc. 4th orthotropic bridge conference. 2015, p. 546–55.
[60] Pijpers R, Pahlavan P, Paulissen J. Structural health monitoring for fatigue life prediction of orthotropic bridge decks. In: Proc. 3rd orthotropic bridge conference. 2013, p. 432–45.
[61] Ono S, Shimozato T, Inaba N, Miki C. Wheel running fatigue test for orthotropic steel bridge decks - IIW doc. XIII-2070-05. Tech. rep., International Institute of Welding; 2005.
[62] Jong FD. Renovation techniques for fatigue cracked orthotropic steel bridge decks [Ph.D. thesis], Delft University of Technology; 2007.
[63] Konda N, Nishio M, Ichimiya M, Kasugai T, Kiyokawa S. Development of fatigue test method and improvement of fatigue life by new functional steel plates for welding of trough rib and deck plate of orthotropic decks. Int J Steel Struct 2013;13:191–7.
[64] Chen Y, Lv P, Li D. Research on fatigue strength for weld structure details of deck with U-rib and diaphragm in orthotropic steel bridge deck. Metals 2019;9:1–15.
[65] Maljaars J, Bonet E, Pijpers R. Fatigue resistance of the deck plate in steel orthotropic deck structures. Eng Fract Mech 2018;201:214–8.
[66] Rodenburg JD, Maljaars J, Hengeveld ST, Vervuurt AH. Tyre contact surface for the fatigue design of orthotropic steel bridge decks. Eng Struct 2023;283:115869.
[67] Pijpers R, Nicoreac M, Wu W, Kolstein M. Fatigue strength determination of the stiffener-to-deck plate weld, weld root crack in 10-20mm deck plate at the cross-beam. Tech. rep., TNO; 2023.
[68] Ya S. Fatigue durability evaluations of trough to deck plate welded details of orthotropic steel deck, doctoral thesis [Ph.D. thesis], Nagoya University; 2009.
[69] Pijpers R, Wu W, Abspoel L, Kolstein M. Fatigue strength determination of the stiffener-to-deck plate weld, with cracks in the weld toe and/or in the weld root. Tech. rep., TNO; 2023.
[70] Wu W, Kolstein H, Veljkovic M. Fatigue resistance of rib-to-deck welded joint in OSDs, analyzed by fracture mechanics. J Construct Steel Res 2019;162:105700.
[71] Bruls A. Measurement and interpretation of dynamic loads in bridges - Phase 3 Fatigue behaviour of orthotropic steel decks - report EUR 13378. Tech. rep., Commission of the European Communities; 1991.
[72] Thonnard J, Janss J. Comportement en fatigue des dalles orthotropes avec raidisseurs trapézoidaux. Tech. rep., CRIF; 1985.
[73] Janss J. Fatigue of welds in orthotropic bridge deck panels with trapezoidal stiffeners. J Constr Steel Res 1988;9:147–54.
[74] Cuninghame J. Fatigue classification of welded joints in orthotropic steel bridge. Transport and Road Research Laboratory; 1990.
[75] Xiao Z-G, Chen T, Zhao X-L. Fatigue strength evaluation of transverse fillet welded joints subjected to bending loads. Int J Fatigue 2012;38:57–64.
[76] Baik B, Yamada K, Ishikawa T. Fatigue strength of fillet welded joint subjected to plate bending. Steel Struct 2008;8:163–9.
[77] Tanaka N, Mori T, Irube T, Miyasita R. Fatigue strength of non load-carrying one side fillet. J Constr Steel Res 1995;3:403–10.
[78] Cuninghame J, Stephens V, Beales C. Measurements and interpretation of dynamic loads in bridges. Final report ECSC 7210-SA/823. Tech. rep., Transport and Road Research Laboratory; 1995.
[79] Maddox SJ. Status review on fatigue performance of fillet welds. J Offshore Mech Arctic Eng 2008;130(3):031006.
[80] Abspoel L, Maljaars J. Fatigue classification of fillet welds in cruciform and T-joints, TNO 2019 R10116B (in Dutch). Tech. rep., TNO; 2019.
[81] Gurney T. Fatigue of steel bridge decks. HMSO Publications Centre; 1992.
[82] Nacher A. Influence of local heating and of surface peening on fatigue behaviour of welded joints and details - IIW doc. XIII-255-1961. Tech. rep., International Institute of Welding; 1961.
[83] Locati L, Bollani G, Massa A. Metallographic influences on Fe 52 carbon steel fatigue strength. Tech. rep., Fiat; 1969.
[84] Sonsino CM, Kaufmann H, Wagener R, Fischer C, Eufinger J. Interpretation of overload effects under spectrum loading of welded high-strength steel joints - IIW-Doc. No. XIII-2315-10/XV-1350-10. Tech. rep., International Institute of Welding; 2010.
[85] Weinert J, Gkatzogiannis S, Engelhardt I, Knoedel P, Ummenhofer T. Application of high frequency mechanical impact treatment to improve the fatigue strength of welded joints in corrosive environment - IIW doc. XIII-2781-19. Tech. rep., International Institute of Welding; 2019.
[86] Newman J, Raju I. Stress intensity factor equations for cracks in three-dimensional finite bodies subjected to tension and bending, technical memorandum 85793. Tech. rep., Nasa; 1970.
[87] Newman J, Raju I. Stress intensity factor equations for cracks in three-dimensional finite bodies subjected to tension and bending, technical memorandum 83200. Tech. rep., Nasa; 1981.
[88] Maddox S, Andrews R. Stress intensity factors for weld toe cracks. In: Proc. computer-aided assessment and control of localized damage. 1990, p. 329–42.
[89] Dijkstra O, Snijder H, VanStraalen I. Fatigue crack growth calculations using stress intensity factors for weld toe geometries. In: Proc. 8th int. conf. offshore mechanics and arctic engineering. OMAE; 1989, p. 137–43.
[90] BS7910:2019. Guide to methods for assessing the acceptability of flaws in metallic structures. BSI; 2019.
[91] Drebenstedt K, Kuhlmann U. Re-evaluation and extension of fatigue test data for welded attachments and butt joints. Ce/Papers 2021;4(2–4):1160–7.
[92] Fukuoka T, Maeda T, Mochizuki K. Effect of plate thickness and improvement by grinding on fatigue strength of cruciform joint under bending. IIW Doc. XIII-2134-06. Tech. rep., International Institute of Welding; 2006.